

# $\rho$ self energy at finite temperature and density in the real-time formalism

Sabyasachi Ghosh and Sourav Sarkar

December 29, 2013

*Theoretical Physics Division, Variable Energy Cyclotron Centre,  
1/AF, Bidhannagar, Kolkata 700064, India*

## Abstract

The  $\rho$  meson self-energy in nuclear matter from baryonic loops is analysed in the real time formulation of field theory at finite temperature and density. The discontinuities across the branch cuts of the self-energy function are evaluated for an exhaustive set of resonances in the loops considering the fully relativistic thermal baryon propagator including anti-baryons. Numerical calculations show a significant broadening of the  $\rho$  spectral function coming from the Landau cut. Adding the contribution from mesonic loops, the full spectral function of the  $\rho$  in a thermal gas of mesons, baryons and antibaryons in equilibrium is evaluated at various values of temperature and baryonic chemical potential.

## 1 Introduction

It is well known that the rate of dilepton production from a thermal system is proportional to the two-point correlation function of vector currents. Hence the spectral function of vector meson, the  $\rho$  meson particular, plays such an important role in the analysis of the late stages of heavy ion collisions [1, 2]. The NA60 experiment at the CERN SPS measured dimuon pairs in In-In collisions in which an excess was observed over the contribution from hadronic decays at freeze-out in the mass region below the  $\rho$  peak [3]. This was attributed to the broadening of the  $\rho$  in hot and dense medium [2]. More recently, the PHENIX experiment reported a substantial excess of electron pairs in the same region of invariant mass [4]. This has been investigated by several groups but the yield in all these cases have remained insufficient to explain the data. Thus the issue of low mass lepton pair yield in heavy ion collisions is far from closed and is one of the key issues to be addressed in the forthcoming Compressed Baryonic Matter(CBM) experiment to be performed at the FAIR facility in GSI [5].

A substantial volume of work has been devoted to the study of  $\rho$  meson properties in hot and dense medium. We do not attempt to review the existing literature but mention a few of them to put our work in perspective. We find that it is only for the  $\pi - \pi$  loop [6, 7] that one calculates the thermal loop directly. In the case of other loops typically involving one heavy and one light particle or both heavy particles one uses in general either the virial formula [8, 9, 10] or the Lindhard function [11, 12, 13, 14, 15]. Most of the calculations involving baryonic effects mentioned above were performed at zero temperature. Finite temperature effects on the  $\rho$  spectral function in dense matter have been evaluated by Rapp et al [12] in terms of resonant interactions of the  $\rho$  with surrounding mesons and baryons in addition to modifying the pion cloud. Eletsky [10] and collaborators have also evaluated the spectral function of vector mesons at finite temperature and density in terms of forward scattering amplitudes constructed using experimental inputs assuming resonance dominance at low energies and a Regge-type approach at higher energies.

The sources modifying the free propagation of a particle find a unified description in terms of contributions from the branch cuts of the self energy function as shown by Weldon [16]. In addition to the unitary cut present already in vacuum, the thermal amplitude generates a new cut, the so called the Landau cut which provides

the effect of collisions with the surrounding particles in the medium. This formalism was applied to obtain the  $\rho$  self-energy in hot mesonic matter [17] by evaluating the one loop self-energies involving the  $\pi$ ,  $\omega$ ,  $h_1$  and  $a_1$  mesons. A significant broadening of the spectral function was obtained without appreciable shift in the mass as expected from chiral interactions.

In this work, we extend this analysis to the case of baryonic matter at finite temperature considering an exhaustive set of 4-star resonances in the baryonic loops making up the  $\rho$  self-energy. The framework of real time thermal field theory [18, 19, 20, 21] that we use, enables us to evaluate the imaginary part of the self-energy from the branch cuts for real and positive values of energy and momentum without having to resort to analytic continuation as in the imaginary time approach [22]. Here we work with the full relativistic baryon propagator in which baryons and anti-baryons manifestly appear on an equal footing. Thus the contributions from all the singularities in the self-energy function including the distant ones coming from the unitary cut of the loops involving heavy baryons are also included. These are usually not considered but can contribute appreciably to the real part of the  $\rho$  meson self-energy as shown [23] in the case of a  $N\Delta$  loop. In addition we have used the covariant form of the momentum dependent vertex functions in the loop integrals in which additional terms [24] required to describe the coupling of off-shell spin 3/2 fields have been introduced.

In the following section we define the correlation function of vector currents and its relation to the transverse propagator of the  $\rho$ . We also provide the various Lagrangian densities which will be used at the vertices of the loop graphs. Next, in section 3 we specify the kinematic decomposition of the thermal propagators. In section 4 we evaluate the baryonic self-energy graphs as well as the discontinuities across the branch cuts. Section 5 contains the results of the numerical evaluation of the real and imaginary parts as well as the  $\rho$  spectral function followed by a summary and discussions in section 6. In the appendix we provide the details of various factors appearing in the expression for self-energy for the different loops and provide some details of evaluation of the imaginary part in addition to a brief discussion on propagators and self-energies in the real time formalism.

## 2 The two point function in the medium

We begin our discussion with the two point function of vector currents in vacuum,

$$T_{\mu\nu}^{ij}(E, \vec{q}) = i \int d^3x d\tau e^{iq \cdot x} \langle 0 | T V_{\mu}^i(x) V_{\nu}^j(0) | 0 \rangle \quad (1)$$

where  $V_{\mu}^i(x)$  are the vector currents of two flavour QCD, given by

$$V_{\mu}^i(x) = \bar{q}(x) \gamma_{\mu} \frac{\tau^i}{2} q(x), \quad q = \begin{pmatrix} u \\ d \end{pmatrix} \quad (2)$$

$\tau^i$  being the Pauli matrices. In the real time formulation of thermal field theory, the in medium two point function assumes a  $2 \times 2$  matrix structure [20]. The thermal two point function is given by

$$T_{\mu\nu}^{ij,ab}(E, \vec{q}) = i \int d^3x d\tau e^{iq \cdot x} \langle T_c V_{\mu}^i(x) V_{\nu}^j(0) \rangle^{ab} \quad (3)$$

where  $\langle \mathcal{O} \rangle$  denotes the ensemble average of an operator  $\mathcal{O}$ ,

$$\langle \mathcal{O} \rangle = Tr(e^{-\beta H} \mathcal{O}) / Tr e^{-\beta H} \quad (4)$$

and  $Tr$  indicating trace over a complete set of states. The superscripts  $a, b (= 1, 2)$  are thermal indices and  $T_c$  denotes time ordering with respect to a contour in the plane of the complex time variable [21]. The two point function of vector currents can be related to the  $\rho$  meson propagator using the method of external fields [25]

where one introduces a classical vector field  $v_\mu^i(x)$  coupled to the vector current  $V_\mu^i(x)$ . The free propagator of the rho meson can be obtained by coupling the external field to the  $\rho$  meson field operator using the Lagrangian [26]

$$\mathcal{L}_{\rho v} = \frac{F_\rho}{m_\rho} \partial^\mu \vec{v}^\nu \cdot (\partial_\mu \vec{\rho}_\nu - \partial_\nu \vec{\rho}_\mu)$$

where  $F_\rho = 154$  MeV is obtained from the decay  $\rho^0 \rightarrow e^+ e^-$ .

The transverse  $\rho$  meson propagator  $G_{\mu\nu}^{ab}$  is then obtained from the relation  $T_{\mu\nu}^{ab} = K_\rho G_{\mu\nu}^{ab}$  where the factor  $K_\rho = (F_\rho q^2 / m_\rho)^2$  comes from the coupling of the current with the  $\rho$  field [17]. The isospin structure is given by  $\delta^{ij}$  which we omit from now on.

The free propagation of the  $\rho$  meson is modified by interactions in the medium which is populated by mesons and baryons. Here we consider one loop graphs shown in Fig. 1 consisting of the nucleon  $N$  and another baryon  $R$  denoted by the double lines. We have included all spin one-half and three-half 4-star resonances listed by the PDG [27] so that  $R$  stands for the  $N^*(1520)$ ,  $N^*(1650)$ ,  $N^*(1700)$ ,  $\Delta(1230)$ ,  $\Delta^*(1620)$ ,  $\Delta^*(1720)$  as well as the  $N(940)$  itself. Omitting isospin factors, the  $\rho N$  couplings with the resonances are described by the gauge invariant interactions [15]

$$\begin{aligned} \mathcal{L} &= \frac{f}{m_\rho} [\bar{\psi}_R \sigma^{\mu\nu} \rho_{\mu\nu} \psi_N + h.c.] & J_R^P &= \frac{1^+}{2} \\ \mathcal{L} &= \frac{f}{m_\rho} [\bar{\psi}_R \sigma^{\mu\nu} \gamma^5 \rho_{\mu\nu} \psi_N + h.c.] & J_R^P &= \frac{1^-}{2} \\ \mathcal{L} &= \frac{f}{m_\rho} [\bar{\psi}_R^\mu \gamma^\nu \gamma^5 \rho_{\mu\nu} \psi_N + h.c.] & J_R^P &= \frac{3^+}{2} \\ \mathcal{L} &= \frac{f}{m_\rho} [\bar{\psi}_R^\mu \gamma^\nu \rho_{\mu\nu} \psi_N + h.c.] & J_R^P &= \frac{3^-}{2} \end{aligned} \quad (5)$$

where  $\rho_{\mu\nu} = \partial_\mu \rho_\nu - \partial_\nu \rho_\mu$  and  $\sigma^{\mu\nu} = \frac{i}{2} [\gamma^\mu \gamma^\nu - \gamma^\nu \gamma^\mu]$ . The isospin part of the  $RN\rho$  interaction is given by

$$\begin{aligned} \bar{\psi}_{Ra} (\vec{\tau} \cdot \rho)_b^a \psi_N^b & \quad I = 1/2 \\ \frac{1}{\sqrt{2}} \bar{\psi}_{Rabc} (\vec{\tau} \cdot \rho)_d^b \psi_N^a \epsilon^{cd} & \quad I = 3/2 \end{aligned} \quad (6)$$

where the indices  $a, b, c, d$  take values 1 and 2 and  $\epsilon^{12} = -\epsilon^{21} = 1$ . For the self-energy diagrams shown in Fig 1, the isospin factor  $I_F$  comes out to be 2 for  $I = \frac{1}{2}$  and  $\frac{4}{3}$  for  $I = \frac{3}{2}$ .

It is essential to point out that for the spin 3/2 resonances this coupling is not quite correct owing to the fact that the free Lagrangian for the Rarita-Schwinger field  $\psi_R^\mu$  has a free parameter [28]. A symmetry is associated with a point transformation under which the free Lagrangian remains invariant up to a change in the value of the parameter [24]. The standard practice is to make a choice of the value of this parameter so that the spin-3/2 propagator has a simple form. In order that the interaction also remains invariant under this transformation an additional term is added to it. Thus the Lagrangians involving spin-3/2 fields take the form

$$\begin{aligned} \mathcal{L} &= \frac{f}{m_\rho} [\bar{\psi}_R^\alpha \mathcal{O}_{\alpha\beta\gamma\nu} \gamma^5 \rho^{\beta\nu} \psi_N + h.c.] & J_R^P &= \frac{3^+}{2} \\ \mathcal{L} &= \frac{f}{m_\rho} [\bar{\psi}_R^\alpha \mathcal{O}_{\alpha\beta\gamma\nu} \rho^{\beta\nu} \psi_N + h.c.] & J_R^P &= \frac{3^-}{2} \end{aligned} \quad (7)$$

with  $\mathcal{O}_{\mu\alpha} = g_{\mu\alpha} - \frac{1}{4} \gamma_\mu \gamma_\alpha$ , the second term contributing only when the spin 3/2 field is off the mass shell. The value of the coupling strength  $f$  thus remains unaffected by this exercise.

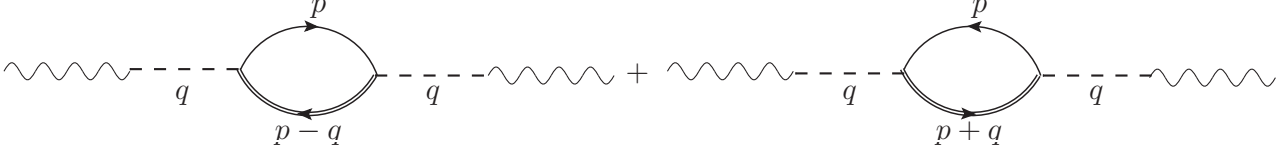


Figure 1: One-loop Feynman diagrams for the two-point function contributing to the  $\rho$  self-energy in baryonic matter. The solid and double lines stand for nucleons and resonances respectively.

### 3 Kinematics of the $\rho$ propagator

The complete propagator of the  $\rho$  is obtained from the Dyson equation [20, 29]

$$G_{\mu\nu}^{ab}(q) = G_{\mu\nu}^{(0)ab}(q) - G_{\mu\lambda}^{(0)ac}(q)\Pi_{\text{tot}}^{\lambda\sigma,cd}(q)G_{\sigma\nu}^{db}(q) \quad (8)$$

where  $\Pi_{\text{tot}}^{\mu\nu,ab}$  denotes the thermal self-energy matrix and  $G_{\mu\nu}^{(0)ab}(q)$  stands for the free thermal propagator.

As described briefly in the appendix, one can get rid of the thermal indices by diagonalisation. In terms of the diagonal elements (denoted by bar) which are analytic functions, the Dyson equation for the  $\rho$  propagator reads

$$\bar{G}_{\mu\nu}(q) = \bar{G}_{\mu\nu}^{(0)}(q) - \bar{G}_{\mu\lambda}^{(0)}(q)\bar{\Pi}_{\text{tot}}^{\lambda\sigma}(q)\bar{G}_{\sigma\nu}(q), \quad (9)$$

where

$$\bar{G}_{\mu\nu}^{(0)}(q) = \left(-g_{\mu\nu} + \frac{q_\mu q_\nu}{q^2}\right) \frac{-1}{q^2 - m_\rho^2 + i\epsilon}. \quad (10)$$

The one loop self energy with baryons is obtained from the two diagrams shown in Fig. 1 so that

$$\bar{\Pi}_B^{\lambda\sigma}(q) = \bar{\Pi}^{\lambda\sigma}(q) + \bar{\Pi}^{\sigma\lambda}(-q). \quad (11)$$

On addition of the contribution from the meson loops the total  $\rho$  self-energy is given by

$$\bar{\Pi}_{\text{tot}}^{\lambda\sigma}(q) = \bar{\Pi}_B^{\lambda\sigma}(q) + \bar{\Pi}_M^{\lambda\sigma}(q). \quad (12)$$

In the medium, the presence of the four velocity  $u_\mu$  introduces an additional scalar variable  $u \cdot q$  in addition to  $q^2$  leading to two independent tensors  $P_{\mu\nu}$  and  $Q_{\mu\nu}$  in terms of which the propagator and self-energy can be written as

$$\begin{aligned} \bar{G}_{\mu\nu} &= P_{\mu\nu}\bar{G}_t + Q_{\mu\nu}\bar{G}_l \\ \bar{\Pi}_{\mu\nu} &= P_{\mu\nu}\bar{\Pi}_t + Q_{\mu\nu}\bar{\Pi}_l \end{aligned} \quad (13)$$

with

$$\begin{aligned} P_{\mu\nu} &= -g_{\mu\nu} + \frac{q_\mu q_\nu}{q^2} - \frac{q^2}{\bar{q}^2}\tilde{u}_\mu\tilde{u}_\nu, \quad \tilde{u}_\mu = u_\mu - (u \cdot q)q_\mu/q^2; \\ Q_{\mu\nu} &= \frac{(q^2)^2}{\bar{q}^2}\tilde{u}_\mu\tilde{u}_\nu, \quad \bar{q}^2 = (u \cdot q)^2 - q^2. \end{aligned} \quad (14)$$

Using (13), the Dyson equation (9) can be solved to get,

$$\bar{G}_t(q) = \frac{-1}{q^2 - m_\rho^2 - \bar{\Pi}_t(q)}, \quad \bar{G}_l(q) = \frac{1}{q^2} \frac{-1}{q^2 - m_\rho^2 - q^2\bar{\Pi}_l(q)} \quad (15)$$

where

$$\bar{\Pi}_t = -\frac{1}{2}(\bar{\Pi}_\mu^\mu + \frac{q^2}{\bar{q}^2}\bar{\Pi}_{00}), \quad \bar{\Pi}_l = \frac{1}{\bar{q}^2}\bar{\Pi}_{00}, \quad \bar{\Pi}_{00} \equiv u^\mu u^\nu \bar{\Pi}_{\mu\nu}. \quad (16)$$

The self-energy function  $\bar{\Pi}_{\mu\nu}$  can be obtained from the 11-component of the in-medium self-energy matrix using (see appendix)

$$\begin{aligned} \text{Re } \bar{\Pi}_{\mu\nu} &= \text{Re } \Pi_{\mu\nu}^{11} \\ \text{Im } \bar{\Pi}_{\mu\nu} &= \epsilon(q_0) \tanh(\beta q_0/2) \text{Im } \Pi_{\mu\nu}^{11} \end{aligned} \quad (17)$$

in terms of which the retarded self-energy is given by [29]

$$\begin{aligned} \text{Re } \Pi_{\mu\nu} &= \text{Re } \bar{\Pi}_{\mu\nu} \\ \text{Im } \Pi_{\mu\nu} &= \epsilon(q_0) \text{Im } \bar{\Pi}_{\mu\nu}. \end{aligned} \quad (18)$$

We now proceed to evaluate the 11-component of the rho self-energy in the following section.

## 4 The self energy and its analytic structure

Let us begin by writing the expression for the  $\rho$  self-energy in vacuum corresponding to the first diagram in Fig. 1. For spin 1/2 resonances in the loop, this is given by

$$\Pi^{\mu\nu}(q) = iI_F \left( \frac{fF(q)}{m_\rho} \right)^2 \int \frac{d^4p}{(2\pi)^4} \text{Tr}[\Gamma^\mu S(p, m_N) \Gamma^\nu S(p-q, m_R)] \quad (19)$$

where  $S(p, m) = (\not{p} + m)\Delta(p, m)$  is the fermion propagator,  $\Delta(p, m)$  being the free propagator for a scalar field of mass  $m$  and is given by

$$\Delta(p, m) = \frac{-1}{p^2 - m^2 + i\epsilon}. \quad (20)$$

Also included is a monopole form factor  $F(q) = \Lambda^2/\Lambda^2 + \bar{q}^2$  with  $\Lambda = 2$  GeV [12] to take into account the finite size of the  $\rho NR$  vertex.

The corresponding expression for the case of loop graphs with spin 3/2 resonances is given by

$$\Pi^{\mu\nu}(q) = iI_F \left( \frac{fF(q)}{m_\rho} \right)^2 \int \frac{d^4p}{(2\pi)^4} \text{Tr}[\Gamma^{\mu\alpha} S(p, m_N) \Gamma^{\nu\beta} S_{\beta\alpha}(p-q, m_R)] \quad (21)$$

where the spin-3/2 propagator is  $S_{\mu\nu}(k, m) = (\not{k} + m)K_{\mu\nu}(k)(\Delta(k, m)$  with  $K_{\mu\nu}(k) = -g_{\mu\nu} + \frac{2}{3m^2}k_\mu k_\nu + \frac{1}{3}\gamma_\mu \gamma_\nu + \frac{1}{3m}(\gamma_\mu k_\nu - \gamma_\nu k_\mu)$ . Obtaining the vertex factors  $\Gamma^\mu$  and  $\Gamma^{\mu\alpha}$  from the interaction Lagrangians (5) and (7) both the expressions (19) and (21) can be expressed in the general form

$$\Pi_{\mu\nu}(q) = i \int \frac{d^4p}{(2\pi)^4} L_{\mu\nu}(p, q) \Delta(p, m_N) \Delta(p-q, m_R) \quad (22)$$

where the factor  $L_{\mu\nu}(p, q)$  consists of the trace over Dirac matrices appearing in the two fermion propagators along with their associated tensor structures, isospin and form factors coming from the  $\rho NR$  vertex. Since the self-energy is transverse,  $L^{\mu\nu}$  can be expressed as

$$L^{\mu\nu}(p, q) = I_F \left( \frac{fF(q)}{m_\rho} \right)^2 [\alpha(p, q)A^{\mu\nu} + \beta(p, q)B^{\mu\nu} + \gamma(p, q)C^{\mu\nu}] \quad (23)$$

where the three gauge-invariant tensors  $A^{\mu\nu}$ ,  $B^{\mu\nu}$  and  $C^{\mu\nu}$  are given by

$$\begin{aligned} A_{\mu\nu}(q) &= -g_{\mu\nu} + q_\mu q_\nu / q^2, \\ B_{\mu\nu}(q, p) &= q^2 p_\mu p_\nu - q \cdot p (q_\mu p_\nu + p_\mu q_\nu) + (q \cdot p)^2 g_{\mu\nu}, \\ C_{\mu\nu}(q, p) &= q^4 p_\mu p_\nu - q^2 (q \cdot p) (q_\mu p_\nu + p_\mu q_\nu) + (q \cdot p)^2 q_\mu q_\nu. \end{aligned} \quad (24)$$

The coefficient functions  $\alpha(p, q)$ ,  $\beta(p, q)$  and  $\gamma(p, q)$  for the different loops are tabulated in the appendix.

We now extend the vacuum self-energy to the nuclear medium. In the real-time version of thermal field theory that we are using the propagators assume the form of matrices. The spin and isospin structure of the self-energy graph remaining the same, it is only the scalar part  $\Delta(p, m)$  of the propagators that assumes a matrix structure. The required 11-component of the fermion propagator is given by

$$E^{11}(p) = \Delta(p) + 2\pi i N(p_0) \delta(p^2 - m^2); \quad N(p_0) = n_+(\omega) \theta(p_0) + n_-(\omega) \theta(-p_0). \quad (25)$$

The function  $n_\pm(\omega) = \frac{1}{e^{\beta(\omega \mp \mu)} + 1}$  is the Fermi distribution where the  $\pm$  sign in the subscript refers to baryons and anti-baryons respectively,  $\omega = \sqrt{p^2 + m^2}$  and  $\mu$  is the baryonic chemical potential which is taken to be equal for all the baryons considered here. Expressed as

$$E^{11}(p) = -\frac{1}{2\omega} \left( \frac{1 - n_+}{p_0 - \omega + i\epsilon} + \frac{n_+}{p_0 - \omega - i\epsilon} - \frac{1 - n_-}{p_0 + \omega - i\epsilon} - \frac{n_-}{p_0 + \omega + i\epsilon} \right) \quad (26)$$

the first and the second terms can be identified with the propagation of baryons above the Fermi sea and holes in the Fermi sea respectively [30] while the third and fourth terms correspond to anti-baryons.

As noted in the previous section, the in-medium self-energy function of the  $\rho$  can be obtained from the 11-component of the thermal self-energy matrix. For the one-loop graphs shown in Fig. 1, the latter is given by

$$\Pi_{\mu\nu}^{11}(q) = i \int \frac{d^4 p}{(2\pi)^4} L_{\mu\nu}(p, q) E^{11}(p, m_N) E^{11}(p - q, m_R). \quad (27)$$

Upon inserting the form of  $E^{11}$  from (25) we get three types of terms. One is the vacuum contribution involving the vacuum parts of the two propagators, the other two being medium dependent, one linear and the other quadratic in the thermal distribution function. Performing the  $p_0$ -integration and using the relations (17) connecting the real and imaginary parts of the 11-component of the self-energy matrix with those of the diagonal element (defined using a bar), the self-energy function is written as

$$\begin{aligned} \bar{\Pi}^{\mu\nu}(q_0, \vec{q}) &= \int \frac{d^3 \vec{p}}{(2\pi)^3 4\omega_N \omega_R} \times \left[ \frac{L_1^{\mu\nu} n_+^N - L_3^{\mu\nu} n_+^R}{q_0 - \omega_N + \omega_R + i\epsilon(q_0)\eta} - \frac{L_2^{\mu\nu} n_-^N - L_4^{\mu\nu} n_-^R}{q_0 + \omega_N - \omega_R + i\epsilon(q_0)\eta} \right. \\ &\quad \left. + \frac{L_1^{\mu\nu} (1 - n_+^N) - L_4^{\mu\nu} n_-^R}{q_0 - \omega_N - \omega_R + i\epsilon(q_0)\eta} - \frac{L_2^{\mu\nu} (1 - n_-^N) - L_3^{\mu\nu} n_+^R}{q_0 + \omega_N + \omega_R + i\epsilon(q_0)\eta} \right] \end{aligned} \quad (28)$$

where  $n^N \equiv n(\omega_N)$  with  $\omega_N = \sqrt{\vec{p}^2 + m_N^2}$ ,  $n^R \equiv n(\omega_R)$  with  $\omega_R = \sqrt{(\vec{p} - \vec{q})^2 + m_R^2}$  and  $L_i^{\mu\nu}$ ,  $i = 1, \dots, 4$  denote the values of  $L^{\mu\nu}(p_0)$  for  $p_0 = \omega_N, -\omega_N, q_0 + \omega_R, q_0 - \omega_R$  respectively.

Let us first consider the imaginary part of the self-energy. The retarded self-energy defined by (18) can be easily read off from the self-energy function (28) to get

$$\begin{aligned} \text{Im}\Pi^{\mu\nu}(q_0, \vec{q}) &= -\pi \coth(\beta q_0/2) \int \frac{d^3 \vec{p}}{(2\pi)^3 4\omega_N \omega_R} \times \\ &\quad [L_1^{\mu\nu} \{(1 - n_+^N - n_-^R)\delta(q_0 - \omega_N - \omega_R) + (n_+^N - n_+^R)\delta(q_0 - \omega_N + \omega_R)\} \\ &\quad + L_2^{\mu\nu} \{(n_-^R - n_-^N)\delta(q_0 + \omega_N - \omega_R) - (1 - n_-^N - n_+^R)\delta(q_0 + \omega_N + \omega_R)\}] \end{aligned} \quad (29)$$

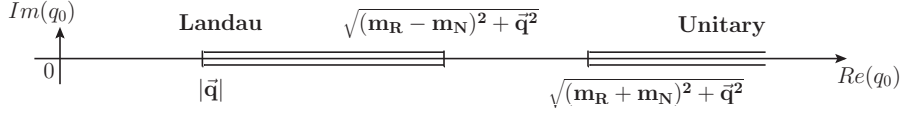


Figure 2: The positions of the Landau and unitary cuts in the complex  $q_0$  plane for  $q^2 > 0$ .

in which the factors  $L_{3,4}^{\mu\nu}$  have converted to  $L_{1,2}^{\mu\nu}$  respectively in association with the  $\delta$ -functions. Following [16, 17] it is interesting to relate the terms appearing in the above expression with scattering and decay processes involving the  $\rho$ , nucleon ( $N$ ) and the heavy resonances ( $R$ ) in the medium. The delta functions in each of the terms in (29) precisely define the kinematic domains where these processes can occur. The regions which are non-vanishing give rise to cuts in the self-energy function. Thus, the first and the fourth terms are non-vanishing for  $q^2 > (m_R + m_N)^2$  giving rise to the unitary cut and second and third terms are non-vanishing for  $q^2 < (m_R - m_N)^2$  giving rise to the Landau cut. Note that the unitary cut is present in vacuum but the Landau cut appears only in the medium.

Consider, for example the first term with  $1 - n_+^N - n_-^R$  in (29). Written as  $(1 - n_+^N)(1 - n_-^R) - n_+^N n_-^R$  this indicates a process in which a (virtual)  $\rho$  decays into a  $NR^{-1}$  pair with the Pauli blocked probability  $(1 - n_+^N)(1 - n_-^R)$  minus the process in which  $NR^{-1}$  pair gets absorbed in the medium with a statistical weight factor  $n_+^N n_-^R$ . This process can obviously take place for  $\rho$ 's with invariant mass ( $\sqrt{q^2}$ )  $> (m_R + m_N)$ , a requirement that is in conformity with the kinematic threshold of the unitary cut coming from the associated  $\delta$ -function.

The kinematic domains where the four terms contribute can be summarised as follows. For  $q_0 > 0$ , the first term in (28) contributes for time-like values of  $q^2$ , the second at space-like  $q^2$  and the third at all  $q^2$ . Likewise, for negative values of the variable  $q_0$ , the second term is non-zero at all  $q^2$ , the third at space-like  $q^2$  and the fourth only for time-like  $q^2$ . In view of the fact that the spectral function of the  $\rho$  will be measured in the invariant mass spectra of lepton pairs we will henceforth confine ourself to the kinematic region  $q_0 > 0$  and  $q^2 > 0$ . The position of the relevant cuts in the complex energy plane for this region are shown in Fig. 2 where we have ignored the portion of the Landau cut for  $q_0 < |\vec{q}|$ . (For a discussion on the branch cuts on the entire  $q_0$  axis, see [17]). Furthermore, we will not include the unitary cut contribution in the imaginary part since the threshold of this cut begins at  $q_0 > m_R + m_N$  which being far away from the  $\rho$  pole is not expected to contribute to the  $\rho$  spectral function in a substantial way. Thus only the Landau cut as given by the third term in eq. (29) will be considered.

Collecting the Landau contributions from both the diagrams using (11) we finally write down the imaginary part of the  $\rho$  self-energy due to baryonic loops

$$\begin{aligned} \text{Im}\Pi_B^{\mu\nu}(q_0, \vec{q}) &= \pi \int \frac{d^3\vec{p}}{(2\pi)^3 2\omega_N} \left[ \frac{L_1^{\mu\nu}(-q)}{2\omega_{R'}} \{ (n_+^N - n_+^{R'}) \delta(q_0 + \omega_N - \omega_{R'}) \} \right. \\ &\quad \left. + \frac{L_2^{\mu\nu}(q)}{2\omega_R} \{ (n_-^N - n_-^R) \delta(q_0 + \omega_N - \omega_R) \} \right] \end{aligned} \quad (30)$$

where  $\omega_{R'} = \sqrt{(\vec{p} + \vec{q})^2 + m_{R'}^2}$ . The two terms in this expression describe the contributions from scattering processes. The factor  $(n_+^N - n_+^{R'})$  expressed as  $(1 - n_+^N)n_+^N - (1 - n_+^N)n_+^{R'}$  can be interpreted as the probability of a  $\rho$  meson scattering on a nucleon from the medium producing a resonance minus the process in which it scatters from the resonance to produce a nucleon, the final states in both cases being Pauli-blocked. The corresponding processes involving anti-baryons are included in the second term.

Let us now proceed to evaluate the integral over the momenta in the  $NR^{-1}$  loop. The integral over  $\cos\theta$  in  $d^3p = -2\pi\sqrt{\omega_N^2 - m_N^2}\omega_N d\omega_N d(\cos\theta)$  is done using the  $\delta$ -function. Also the condition  $|\cos\theta| \leq 1$  puts

restriction on the range of integration over  $\omega_N$ . A substantial simplification is obtained by changing the integration variable to  $x$  using  $\omega_N = \frac{S^2}{2q^2}(-q_0 + |\vec{q}|x)$  where  $S^2 = q^2 - m_R^2 + m_N^2$  to get

$$\text{Im}\Pi_B^{\mu\nu}(q_0, \vec{q}) = -\frac{S^2}{32\pi q^2} \int_{-W}^W dx L^{\mu\nu}(x) \{n_+(q_0 + \omega_N) - n_+(\omega_N) + n_-(q_0 + \omega_N) - n_-(\omega_N)\} \quad (31)$$

where  $W = \sqrt{1 - 4q^2 m_N^2 / S^4}$  and the factor  $L^{\mu\nu}$  in terms of the variable  $x$  has the same form for both diagrams in Fig. 1. This is shown in the appendix.

The real part consists of principal value integrals which remain after removing the imaginary part from (28). Note that unlike the imaginary part, the real part of the self-energy at a given value of  $q$  receives contribution from all the four terms.

Up to now we have been treating the baryon resonances  $R$  in the narrow width approximation. It is indeed necessary to consider the width of the unstable baryons in a realistic evaluation of the spectral function. For this, we follow the procedure (see e.g. [31, 32]) of convoluting the self energy calculated in the narrow width approximation with the spectral function of the baryons. This approach has the advantage that the analytic structure of the self energy discussed above remains undisturbed.

$$\Pi_B^{\mu\nu}(q; m_R) = \frac{1}{N_R} \int_{m_R - 2\Gamma_R}^{m_R + 2\Gamma_R} dM \frac{1}{\pi} \text{Im} \left[ \frac{1}{M - m_R + \frac{i}{2}\Gamma_R(M)} \right] \Pi_B^{\mu\nu}(q; M) \quad (32)$$

with  $N_R = \int_{m_R - 2\Gamma_R}^{m_R + 2\Gamma_R} dM \frac{1}{\pi} \text{Im} \left[ \frac{1}{M - m_R + \frac{i}{2}\Gamma_R(M)} \right]$  and  $\Gamma_R(M) = \Gamma_{R \rightarrow N\pi}(M) + \Gamma_{R \rightarrow N\rho}(M)$ . As a consequence of this convolution, the sharp ends of the regions of non-zero imaginary part smoothly go to zero at a higher value of  $M$  depending upon the width of the resonance. This is shown in Fig. 3 for the  $N^*(1520)$  resonance.

Nuclear medium at finite temperature is also substantially populated by mesons which modify the  $\rho$  propagation in the medium in a non-trivial way. This has been studied [17] following the same procedure as described here for mesonic loop graphs with one internal pion line and another meson line  $h$  where  $h = \pi, \omega, h_1, a_1$  using interactions from chiral perturbation theory. Collecting the real and imaginary parts, the self-energy from mesonic loops can be written as

$$\begin{aligned} \Pi_M^{\mu\nu}(q_0, \vec{q}) = & \int \frac{d^3\vec{k}}{(2\pi)^3} \frac{1}{4\omega_\pi\omega_h} \left[ -\frac{N_1^{\mu\nu}n_\pi - N_3^{\mu\nu}n_h}{q_0 - \omega_\pi + \omega_h + i\epsilon(q_0)\eta} + \frac{N_2^{\mu\nu}n_\pi - N_4^{\mu\nu}n_h}{q_0 + \omega_\pi - \omega_h + i\epsilon(q_0)\eta} \right. \\ & \left. + \frac{N_1^{\mu\nu}(1 + n_\pi) + N_4^{\mu\nu}n_h}{q_0 + \omega_\pi - \omega_h + i\epsilon(q_0)\eta} - \frac{N_2^{\mu\nu}(1 + n_\pi) + N_3^{\mu\nu}n_h}{q_0 + \omega_\pi + \omega_h + i\epsilon(q_0)\eta} \right] \quad (33) \end{aligned}$$

where the Bose distribution functions  $n_\pi \equiv n(\omega_\pi)$  with  $\omega_\pi = \sqrt{\vec{k}^2 + m_\pi^2}$  and  $n_h \equiv n(\omega_h)$  with  $\omega_h = \sqrt{(\vec{q} - \vec{k})^2 + m_h^2}$ .  $N_i^{\mu\nu}$  ( $i = 1, 4$ ) are the values of  $N^{\mu\nu}(k_0)$  for  $k_0 = \omega_\pi, -\omega_\pi, q_0 + \omega_h, q_0 - \omega_h$  respectively and can be expressed in terms of the gauge-invariant tensors (24). The complete expressions are provided in the appendix. Using the procedure described above we have improved upon the calculations in [17] by including the width of the heavy mesons  $a_1$  and  $h_1$ . In this case we use a slightly different formula [32],

$$\Pi_M^{\mu\nu}(q; m_h) = \frac{1}{N_h} \int_{(m_h - 2\Gamma_h)^2}^{(m_h + 2\Gamma_h)^2} dM^2 \frac{1}{\pi} \text{Im} \left[ \frac{1}{M^2 - m_h^2 + iM\Gamma_h(M)} \right] \Pi_M^{\mu\nu}(q; M) \quad (34)$$

with  $N_h = \int_{(m_h - 2\Gamma_h)^2}^{(m_h + 2\Gamma_h)^2} dM^2 \frac{1}{\pi} \text{Im} \left[ \frac{1}{M^2 - m_h^2 + iM\Gamma_h(M)} \right]$  and  $\Gamma_h(M) = \Gamma_{h \rightarrow \rho\pi}(M)$ .

The transverse and longitudinal components can then be obtained from the self-energy tensors using the relations (16).



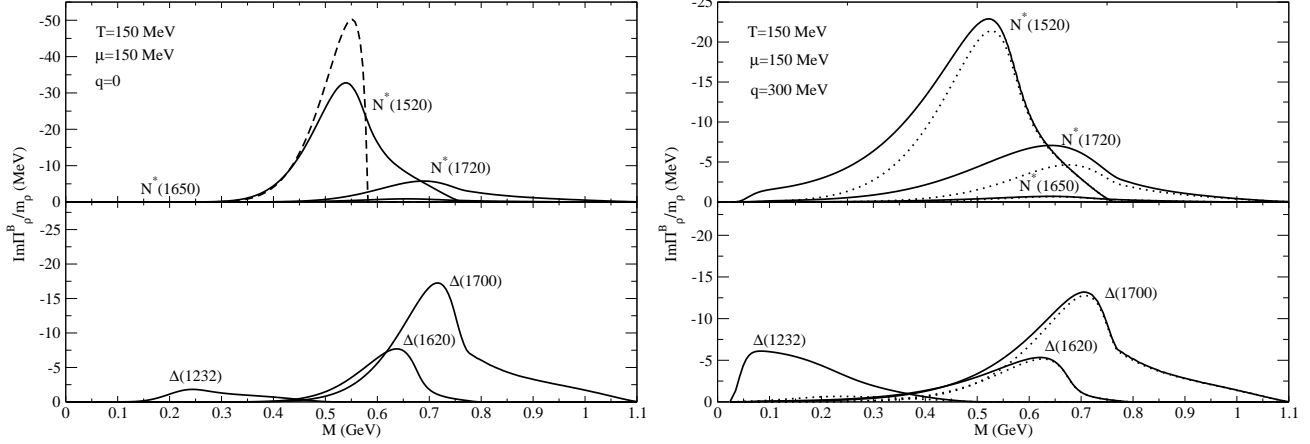


Figure 3: Imaginary part of  $\rho$  meson self-energy showing the individual contributions for different  $NR$  loops. Left panel shows results for  $\vec{q} = 0$  and the right panel shows the transverse (solid) and longitudinal (dotted) parts for  $\vec{q} = 300$  MeV. The long dashed line in the upper panel on the left shows the imaginary part of the  $NN^*(1520)$  loop evaluated in the narrow width approximation.

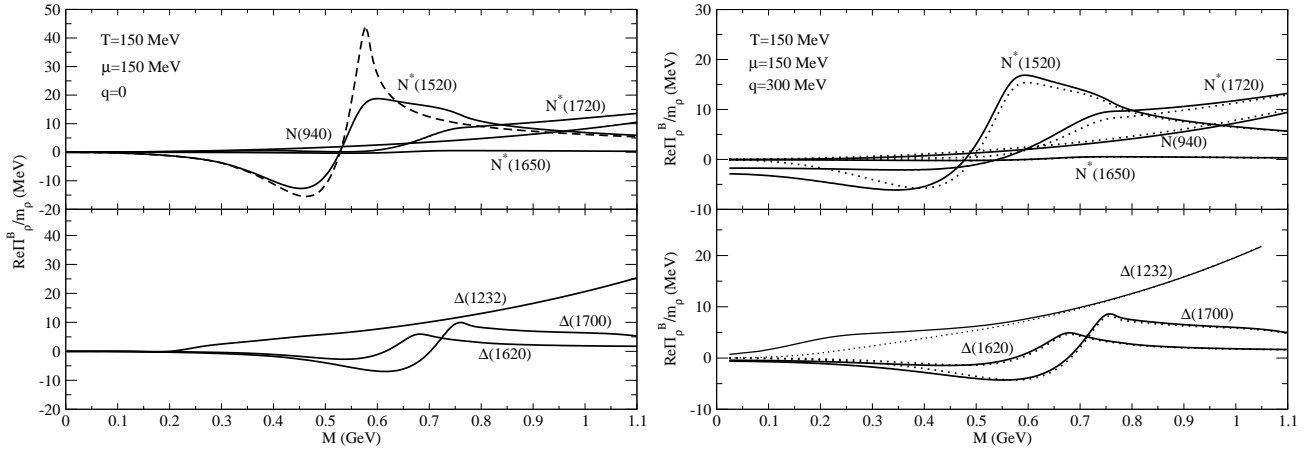


Figure 4: Same as Fig. 3 for the real part

## 5 Numerical Results

In this section we present the results of numerical evaluation beginning with the imaginary part of the  $\rho$  self-energy as a function of the invariant mass  $\sqrt{q^2} \equiv M$  for two values of the three momentum. The Landau cut contribution starts from  $M = 0$  for all values of the three momentum. Shown in Fig. 3 left panel are the contributions from the individual  $NR$  loops for a  $\rho$  meson at rest. The  $NN^*(1520)$  loop makes the most significant contribution followed by the  $N^*(1720)$  and  $\Delta(1700)$ . The right panel shows the corresponding results for  $\vec{q} = 300$  MeV where the transverse and longitudinal components  $\Pi_t$  and  $q^2\Pi_l$  have been shown separately by solid and dotted lines respectively. (Note that for a  $\rho$  meson at rest  $\Pi_t = q_0^2\Pi_l$ .) The corresponding results for the thermal contribution to the real part are shown in Fig. 4. The divergent vacuum contribution in this case is assumed to renormalize the  $\rho$  mass to its physical value. Also shown by the long dashed lines in the left upper panels of Figs. 3 and 4 are the corresponding contributions to the real and imaginary parts coming from the  $NN^*(1520)$  loop computed in the narrow width approximation.

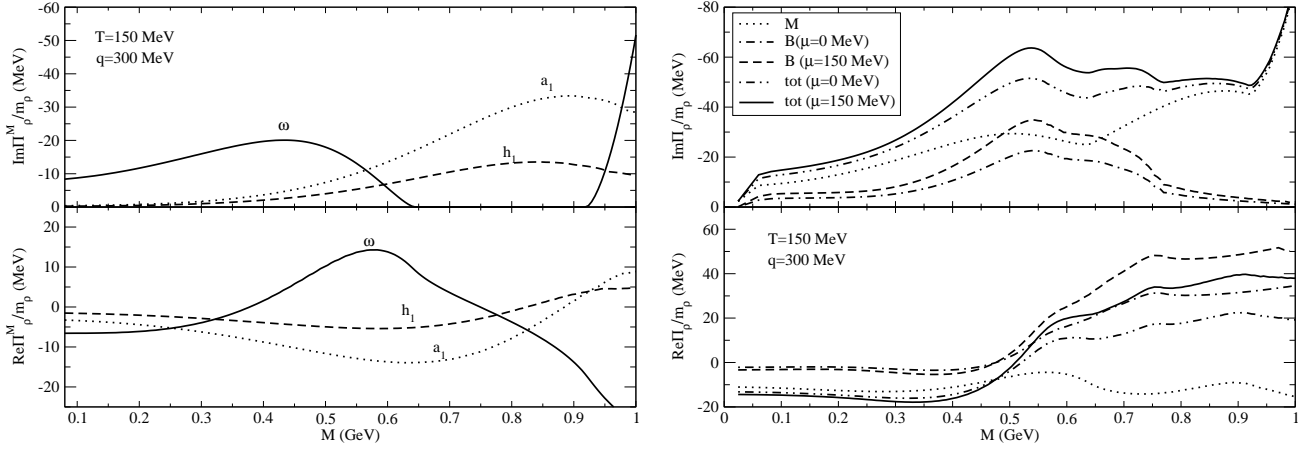


Figure 5: (Left) Imaginary and real parts of  $\rho$  meson self-energy showing the individual contributions for different  $\pi - h$  loops. (Right) The total contribution from meson and baryon loops.

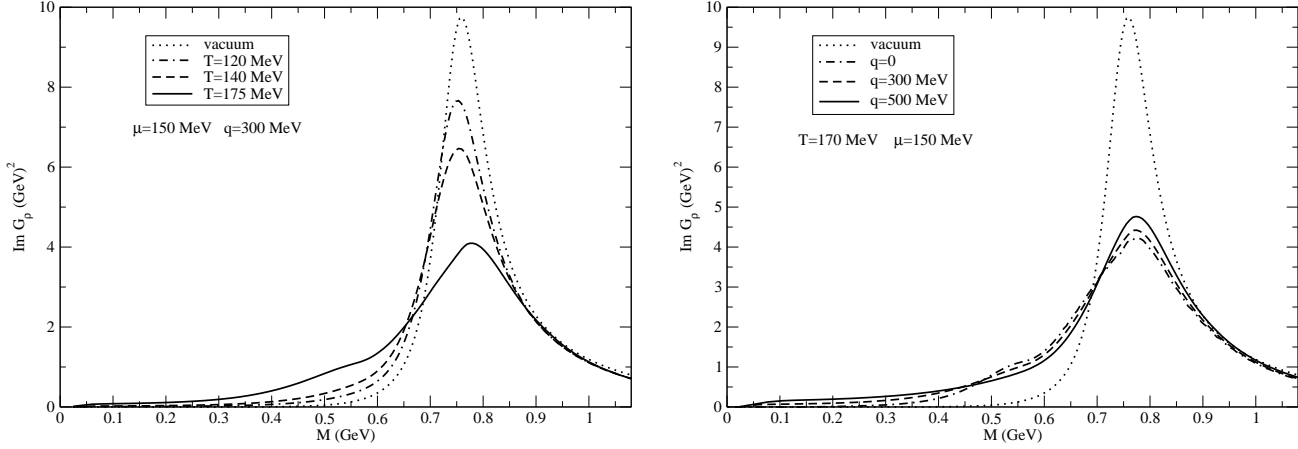


Figure 6: The spectral function of the  $\rho$  meson for (left) different values of the temperature  $T$  and (right) different values of the three-momentum  $\vec{q}$ .

Next we show the results of the spin-averaged  $\rho$  self-energy defined by

$$\Pi = \frac{1}{3}(2\Pi_t + q^2\Pi_l) . \quad (35)$$

where the transverse and longitudinal components are obtained using (16). In Fig. 5 left panel the imaginary and real parts of  $\pi - h$  loop graphs are shown in the upper and lower panels respectively. The Landau and unitary cut contributions for the  $\pi - \omega$  loop are clearly discernible though the contribution at the  $\rho$  pole is dominated by the  $a_1$ . On the right panel we plot the total contribution from the baryon and meson loops for two values of the baryonic chemical potential. The small positive contribution from the baryon loops to the real part is partly compensated by the negative contributions from the meson loops. The substantial baryon contribution at vanishing baryonic chemical potential reflects the importance of anti-baryons.

We now turn to the spin averaged spectral function given by

$$\text{Im} \bar{G}(q) = \frac{1}{3}(2\text{Im} \bar{G}_t + q^2\text{Im} \bar{G}_l) \quad (36)$$

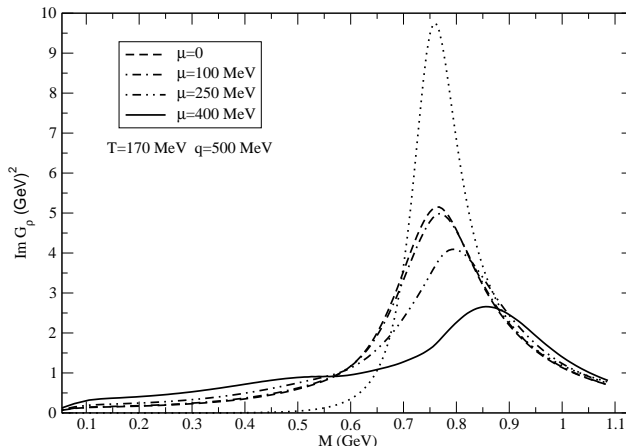


Figure 7: The spectral function of the  $\rho$  meson for different values of the baryonic chemical potential  $\mu$

where

$$\text{Im} \bar{G}_{t,l}(q) = \frac{-\sum \text{Im} \bar{\Pi}_{t,l}^{\text{tot}}}{(M^2 - m_\rho^2 - (1, q^2) \sum \text{Re} \bar{\Pi}_{t,l}^{\text{tot}})^2 + \{(1, q^2) \sum \text{Im} \bar{\Pi}_{t,l}^{\text{tot}}\}^2}. \quad (37)$$

First, in Fig.6 left panel we plot the spectral function at fixed values of the baryonic chemical potential and three-momentum for various representative values of the temperature. We observe an increase of spectral strength at lower invariant masses resulting in broadening of the spectral function with increase in temperature. This is purely a Landau cut contribution from the baryonic loops arising from the scattering of the  $\rho$  from baryons in the medium. However, we do not observe much variation with the three-momentum of the  $\rho$  as seen from the figure on the right panel.

We then plot in Fig. 7, the spectral function for various values of the baryonic chemical potential for a fixed temperature. For high values of  $\mu$  we observe an almost flattened spectral density of the  $\rho$ .

Owing to differences in the various approaches to the evaluation of the  $\rho$  spectral function followed in the literature, a direct numerical comparison with earlier results does not appear to be meaningful. These differences are at the level of the basic formulae arising from the type of couplings of the nucleon and the rho fields with the various baryon resonances considered as well as in the form of the propagators used in the calculations. There also exist differences at the level of formalism employed in the evaluation of the  $\rho$  self-energy. We thus end this section by showing how the in-medium spectral function of the  $\rho$  is manifested in the dilepton emission rate. This rate from thermalised hadronic matter is given by [33]

$$\frac{dR}{d^4q} = -\frac{\alpha^2}{3\pi^3 q^2} H(M^2) n_{BE}(q_0) g^{\mu\nu} \text{Im} T_{\mu\nu}(q_0, \vec{q}) \quad (38)$$

where  $\text{Im} T_{\mu\nu}$  is the imaginary part of the (retarded) two-point function of vector currents which can be obtained from (3) using relations analogous to (17). The quantity  $H(M^2) = (1 + 2m_l^2/M^2) (1 - 4m_l^2/M^2)^{1/2}$  is of the order of unity for electrons and will be omitted henceforth. In the low invariant mass ( $M$ ) region,  $\text{Im} T_{\mu\nu}$  is usually expressed as a sum over the spectral densities of the vector mesons  $\rho$ ,  $\omega$  and  $\phi$  [1]. This is however justified only in vacuum. The vector mesons  $\rho$  and  $\omega$  can in general undergo mixing in the presence of matter which can lead to non-trivial modifications, for example, of the electromagnetic form factor of the pion [34] and consequently the invariant mass distribution of lepton pairs. In the following, we will consider only the  $\rho$  pole contribution which is known to play the most dominant role. The dilepton rate in this case can be expressed in terms of the spin-averaged spectral function of the  $\rho$  (36) getting,

$$\frac{dR}{dM^2 dq_T dq_T dy} = \frac{\alpha^2}{\pi^2 M^2} n_{BE}(q_0) K_\rho \text{Im} \bar{G}(q_0, \vec{q}) \quad (39)$$

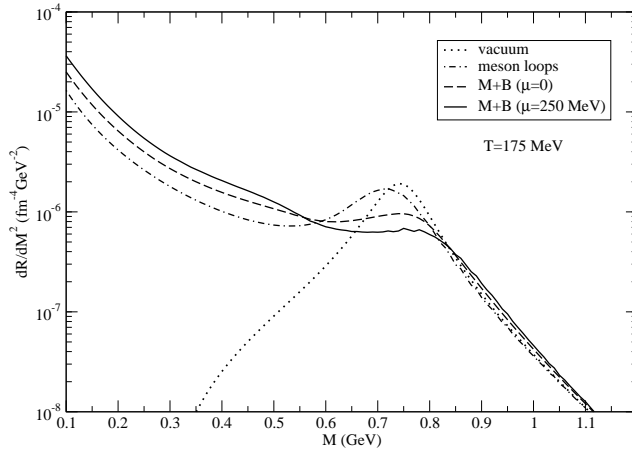


Figure 8: The lepton pair emission rate at  $T = 175$  MeV with and without baryon (B) loops in addition to the meson (M) loops

where we have used  $T_{\mu\nu} = K_\rho G_{\mu\nu}$  as defined earlier. Integrating over the transverse momentum  $q_T$  and rapidity  $y$  of the electron pairs we plot  $dR/dM^2$  vs  $M$  in Fig. 8 for  $T=175$  MeV. Because of the kinematical factors multiplying the  $\rho$  spectral function the broadening appears magnified in the dilepton emission rate. A significant enhancement is seen in the low mass lepton production rate due to baryonic loops over and above the mesonic ones shown by the dot-dashed line. The substantial contribution from baryonic loops even for vanishing chemical potential points to the important role played by antibaryons in thermal equilibrium in systems created at RHIC and LHC energies.

## 6 Summary and Discussion

We evaluate the  $\rho$  self-energy to one loop in nuclear matter at finite temperature and baryon density. Loop graphs involving the nucleon and 4-star  $N^*$  and  $\Delta$  resonances up to spin 3/2 were calculated using gauge invariant interactions in the framework of real time thermal field theory to obtain the correct relativistic expressions for the  $\rho$  self-energy. The singularities in the complex energy plane were analysed and the imaginary part obtained from the Landau cut contribution. Results for the real and imaginary parts at non-zero three-momenta for various values of temperature and baryonic chemical potential were shown for the individual loop graphs. Adding the contributions from mesons obtained in the same formalism, the spectral function of the  $\rho$  was observed to undergo a significant modification at and below the nominal rho mass which was seen to bring about a large enhancement of lepton pair yield in this region.

It may be emphasised that the determination of the  $\rho$  spectral density at finite temperature and baryon density by an explicit evaluation of loop graphs using thermal field theoretic techniques such as performed here is of relevance in view of precision data from experiments at RHIC and LHC as well as from the FAIR facility at GSI in future. But an actual comparison with data will involve a space-time evolution of the static rates using a framework like relativistic hydrodynamics. Efforts in this direction are in progress and will be reported in due course.

## 7 Acknowledgement

The authors gratefully acknowledge discussions with S. Mallik during the course of this work and to J. Alam for useful suggestions.

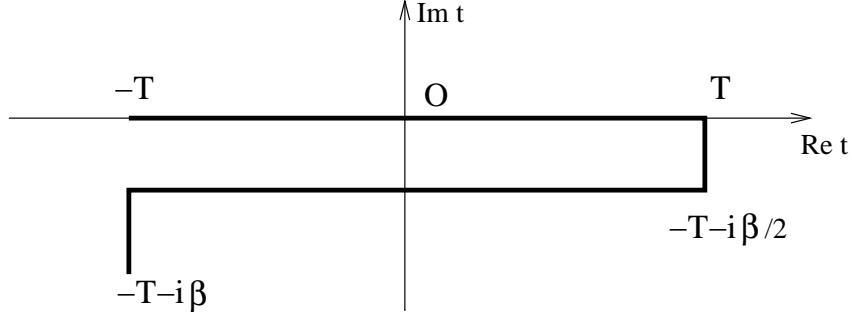


Figure 9: Contour in the complex time plane for real time formalism

## 8 Appendix

### 8.1 The real-time propagators and the self-energy matrix

In the real time formulation of thermal field theory a two-point function of local operators assumes a  $2 \times 2$  matrix structure on account of the shape of the contour in the complex time plane. Thus the current correlator  $T^{\mu\nu}$  [35] as well as propagators for various fields[20] assume a matrix structure. For the contour shown in Fig. 9 the components of a free scalar propagator are as

$$\begin{aligned} D^{11} &= -(D^{22})^* = \Delta(q) + 2\pi i n \delta(q^2 - m^2) \\ D^{12} &= D^{21} = 2\pi i \sqrt{n(1+n)} \delta(q^2 - m^2) \end{aligned} \quad (\text{A.1})$$

where  $\Delta(q)$  is the Feynman propagator in vacuum,

$$\Delta(q^2) = \frac{-1}{q^2 - m^2 + i\epsilon}. \quad (\text{A.2})$$

The thermal propagator may be diagonalised in the form

$$D^{ab}(q_0, \vec{q}) = U^{ac}(q_0) [\text{diag}\{\Delta(q_0, \vec{q}), -\Delta^*(q_0, \vec{q})\}]^{cd} U^{db}(q_0) \quad (\text{A.3})$$

with the elements of the diagonalising matrix as

$$U^{11} = U^{22} = \sqrt{1+n}, \quad U^{12} = U^{21} = \sqrt{n}.$$

Using the (transverse) vector propagator given by

$$G_{\mu\nu}^{(0)ab}(q) = \left( -g_{\mu\nu} + \frac{q_\mu q_\nu}{q^2} \right) D^{ab}(q) \quad (\text{A.4})$$

in the Dyson equation and the fact that  $U$  diagonalises not only the free propagator, but also the complete one [20, 21] it turns out that the self-energy matrix  $\Pi_{\mu\nu}^{ab}$  is also diagonalisable by  $(U^{-1})^{ab}$ ,

$$\Pi_{\mu\nu}^{ab}(q) = [U^{-1}(q_0)]^{ac} [\text{diag}\{\bar{\Pi}_{\mu\nu}(q), -\bar{\Pi}_{\mu\nu}^*(q)\}]^{cd} [U^{-1}(q_0)]^{db}. \quad (\text{A.5})$$

The relations

$$\begin{aligned} \text{Re } \bar{\Pi}_{\mu\nu} &= \text{Re } \Pi_{\mu\nu}^{11} \\ \text{Im } \bar{\Pi}_{\mu\nu} &= \epsilon(q_0) \tanh(\beta q_0/2) \text{Im } \Pi_{\mu\nu}^{11} \end{aligned} \quad (\text{A.6})$$

trivially follow showing that the thermal matrices are actually given by a *single* analytic function which essentially coincides with the corresponding result from the imaginary time formulation.

$R$	$J^P$	$f$	$\alpha$	$\beta$	$\gamma$
$N(940)$	$\frac{1}{2}^+$	7.7	$\frac{1}{2}\alpha_{1/2+}$	$\frac{1}{2}\beta_{1/2}$	$\frac{1}{2}\gamma_{1/2}$
$N^*(1520)$	$\frac{3}{2}^-$	7.0	$\alpha_{3/2-}$	$\beta_{3/2}$	$\gamma_{3/2}$
$N^*(1650)$	$\frac{1}{2}^-$	0.9	$\alpha_{1/2-}$	$\beta_{1/2}$	$\gamma_{1/2}$
$N^*(1720)$	$\frac{3}{2}^+$	7.0	$\alpha_{3/2+}$	$\beta_{3/2}$	$\gamma_{3/2}$
$\Delta(1232)$	$\frac{3}{2}^+$	10.5	$\alpha_{3/2+}$	$\beta_{3/2}$	$\gamma_{3/2}$
$\Delta(1620)$	$\frac{1}{2}^-$	2.7	$\alpha_{1/2-}$	$\beta_{1/2}$	$\gamma_{1/2}$
$\Delta(1700)$	$\frac{3}{2}^-$	5.0	$\alpha_{3/2-}$	$\beta_{3/2}$	$\gamma_{3/2}$

Table 1: Table showing the coefficients  $\alpha$ ,  $\beta$  and  $\gamma$  for loops containing the various resonances considered.

## 8.2 The factor $L^{\mu\nu}$ in baryonic loops

The factor  $L^{\mu\nu}$  which appears in the loop integrals is given by

$$L^{\mu\nu}(p, q) = I_F \left( \frac{fF(q)}{m_\rho} \right)^2 [\alpha A^{\mu\nu} + \beta B^{\mu\nu} + \gamma C^{\mu\nu}] \quad (\text{A.7})$$

where  $A^{\mu\nu}$ ,  $B^{\mu\nu}$  and  $C^{\mu\nu}$  are the transverse tensors defined in (24). The coefficient factors  $\alpha$ ,  $\beta$ ,  $\gamma$  are given in Table 1 where

$$\begin{aligned}
\alpha_{1/2+} &= 4q^2(p^2 - m_N m_R + p \cdot q) \\
\alpha_{1/2-} &= \alpha_{1/2+}(m_N \rightarrow -m_N) \\
\beta_{1/2} &= 8 \\
\gamma_{1/2} &= 0 \\
\alpha_{3/2+} &= \frac{2q^2}{3m_R^2} [p^2(p^2 - 3q^2) + p \cdot q(3p^2 + q^2) \\
&\quad + 3m_R^2(p^2 + 2m_N m_R + p \cdot q) \\
&\quad - 2m_N m_R(p^2 + q^2 - 2p \cdot q)] \\
\alpha_{3/2-} &= \alpha_{3/2+}(m_N \rightarrow -m_N) \\
\beta_{3/2} &= 4(1 + p^2/3m_R^2) \\
\gamma_{3/2} &= -4/3m_R^2.
\end{aligned} \quad (\text{A.8})$$

The corresponding expressions of  $\alpha$ ,  $\beta$  and  $\gamma$  for the second graph of Fig. 1 can be obtained by replacing  $q \rightarrow -q$  as indicated in (11). The factor 1/2 in front of the coefficients for the  $NN$  loop is put to prevent a

double counting of this contribution. The coupling constants  $f$  have been obtained as in [13, 15]. The values are also in reasonable agreement as seen in Table 1.

A considerable simplification in the imaginary part can be achieved in the sum of the two diagrams in Fig. 1 by a change of variables. Note that only the factor  $p \cdot q$  which appears with various powers in the tensors  $A^{\mu\nu}$ ,  $B^{\mu\nu}$  and  $C^{\mu\nu}$  and in the factors  $\alpha$  takes on different values in the various terms in the expression for the imaginary part of self energy. We recall for convenience the imaginary part coming from first diagram in Fig. 1,

$$\begin{aligned} \text{Im}\bar{\Pi}^{(1)}(q_0, \vec{q}) &= -\pi \int \frac{d^3\vec{p}}{(2\pi)^3 4\omega_N\omega_R} \times \\ &[L_1(q)\{(1 - n_+^N - n_-^R)\delta(q_0 - \omega_N - \omega_R) + (n_+^N - n_+^R)\delta(q_0 - \omega_N + \omega_R)\} \\ &+ L_2(q)\{(n_-^R - n_-^N)\delta(q_0 + \omega_N - \omega_R) - (1 - n_-^N - n_+^R)\delta(q_0 + \omega_N + \omega_R)\}] \end{aligned} \quad (\text{A.9})$$

where we have dropped the Lorentz indices for brevity. For the first two terms  $p_0 = \omega_N$  and on integration over the angle using either of the two delta functions one has  $\vec{p} \cdot \vec{q} = -\frac{1}{2}(S^2 - 2q_0\omega_N)$  with  $S^2 = q^2 - m_R^2 + m_N^2$ . One thus gets  $p \cdot q = p_0q_0 - \vec{p} \cdot \vec{q} = \frac{S^2}{2}$ . Changing variable to  $x$  using  $\omega_N = \frac{S^2}{2q^2}(q_0 + |\vec{q}|x)$  one has

$$A_\mu^\mu = -3, \quad A_{00} = \frac{|\vec{q}|^2}{q^2} \quad (\text{A.10})$$

$$B_\mu^\mu = m_\pi^2 q^2 + \frac{S^4}{2}, \quad B_{00} = -\frac{|\vec{q}|^2 S^4}{4q^2}(1 - x^2) \quad (\text{A.11})$$

$$C_\mu^\mu = q^2(m_\pi^2 q^2 - \frac{S^4}{4}), \quad C_{00} = \frac{|\vec{q}|^2 S^4}{4} x^2. \quad (\text{A.12})$$

For the last two terms,  $\vec{p} \cdot \vec{q} = -\frac{1}{2}(S^2 + 2q_0\omega_N)$  and  $p_0 = -\omega_N$  so that here too  $p \cdot q = \frac{S^2}{2}$ . Defining  $x$  in this case through  $\omega_N = \frac{S^2}{2q^2}(-q_0 + |\vec{q}|x)$  one recovers the same expression for the tensor component as in the first two terms.

The corresponding expression for the imaginary part from the second graph of Fig. 1 is obtained by changing  $q \rightarrow -q$  in the expression for  $\text{Im}\bar{\Pi}$  given by (A.9) getting

$$\begin{aligned} \text{Im}\bar{\Pi}^{(2)}(q_0, \vec{q}) &= -\pi \int \frac{d^3\vec{p}}{(2\pi)^3 4\omega_N\omega_{R'}} \times \\ &[L_2(-q)\{(1 - n_+^N - n_+^{R'})\delta(q_0 - \omega_N - \omega_{R'}) + (n_-^N - n_-^{R'})\delta(q_0 - \omega_N + \omega_{R'})\} \\ &+ L_1(-q)\{(n_+^{R'} - n_+^N)\delta(q_0 + \omega_N - \omega_{R'}) - (1 - n_+^N - n_-^{R'})\delta(q_0 + \omega_N + \omega_{R'})\}] \end{aligned} \quad (\text{A.13})$$

where  $\omega_{R'} = \sqrt{(\vec{p} + \vec{q})^2 + m_{R'}^2}$ . In this case, for the first two terms  $\vec{p} \cdot \vec{q} = \frac{1}{2}(S^2 - 2q_0\omega_N)$  which along with  $p_0 = -\omega_N$  gives  $p \cdot q = -\frac{S^2}{2}$ . The same is obtained for the last two terms for which  $\vec{p} \cdot \vec{q} = \frac{1}{2}(S^2 + 2q_0\omega_N)$  and  $p_0 = \omega_N$ . Making a change of variables as before, identical values of the tensor components are obtained as in (A.12) as a consequence of the fact that the gauge invariant tensors  $A_{\mu\nu}$ ,  $B_{\mu\nu}$  and  $C_{\mu\nu}$  are even under  $q \rightarrow -q$ . The coefficients  $\alpha$ ,  $\beta$  and  $\gamma$  also remain unchanged in the two diagrams the sign of  $p \cdot q$  in the expressions remaining the same under the combined effect of  $q \rightarrow -q$  and a reversal in its magnitude ( $\frac{S^2}{2} \rightarrow -\frac{S^2}{2}$ ). The value of  $L(x)$  thus comes out to be the same for all cases and we end up with the final expression given by (31).

### 8.3 Expressions for $N_{\mu\nu}$ for mesonic loops

The expressions for  $N_{\mu\nu}$  appearing in the  $\rho$  self-energy (33) for  $\pi - h$  loops have been obtained in [17] and are given below,

$$\begin{aligned}
N_{\mu\nu}^{(\pi)}(q, k) &= \left( \frac{2G_\rho}{m_\rho F_\pi^2} \right)^2 C_{\mu\nu} \\
N_{\mu\nu}^{(\omega)}(q, k) &= -4 \left( \frac{g_1}{F_\pi} \right)^2 (B_{\mu\nu} + q^2 k^2 A_{\mu\nu}) \\
N_{\mu\nu}^{(h_1)}(q, k) &= - \left( \frac{g_2}{F_\pi} \right)^2 \left( B_{\mu\nu} - \frac{1}{m_{h_1}^2} C_{\mu\nu} \right) \\
N_{\mu\nu}^{(a_1)}(q, k) &= -2 \left( \frac{g_3}{F_\pi} \right)^2 \left( B_{\mu\nu} - \frac{1}{m_{a_1}^2} C_{\mu\nu} \right)
\end{aligned} \tag{A.14}$$

where the constants  $G_\rho = 69$  MeV,  $F_\pi = 93$  MeV,  $g_1 = 0.87$ ,  $g_2 = 1.0$  and  $g_3 = 1.1$ . These can be simplified as shown above and finally expressed in terms of the tensor components defined in (A.12). As in the case of baryon loops the factors  $N_{\mu\nu}$  have also been multiplied by the square of the monopole form factor  $F(q)$  defined earlier.

## References

- [1] J. Alam, S. Sarkar, P. Roy, T. Hatsuda and B. Sinha, *Annals Phys.* **286** (2001) 159
- [2] R. Rapp and J. Wambach, *Adv. Nucl. Phys.* **25**, 1 (2000)
- [3] R. Arnaldi, et al (NA60 Collaboration), *Eur. Phys. J.* **C61**, 711 (2009).
- [4] A. Adare *et al.* [PHENIX Collaboration], *Phys. Rev. C* **81** (2010) 034911
- [5] [http://www.gsi.de/forschung/fair\\_experiments/CBM/1intro\\_e.html](http://www.gsi.de/forschung/fair_experiments/CBM/1intro_e.html)
- [6] C. Gale and J. I. Kapusta *Nucl. Phys.* **B357**, 65 (1991)
- [7] M. Herrmann, B. L. Friman and W. Norenberg, *Nucl. Phys. A* **560** (1993) 411.
- [8] H. Leutwyler and A. Smilga, *Nucl. Phys.* **B 342**, 302 (1990)
- [9] M. Post, S. Leupold and U. Mosel, *Nucl. Phys. A* **689** (2001) 753
- [10] V. L. Eletsky, M. Belkacem, P. J. Ellis and J. I. Kapusta, *Phys. Rev. C* **64** (2001) 035202
- [11] A. L. Fetter and J. D. Walecka, *Quantum Theory of many-Particle Systems* (Dover, New York, 2003), p 158.
- [12] R. Rapp, G. Chanfray and J. Wambach, *Nucl. Phys. A* **617**, 472 (1997)
- [13] W. Peters, M. Post, H. Lenske, S. Leupold and U. Mosel, *Nucl. Phys. A* **632**, 109 (1998)
- [14] D. Cabrera, E. Oset and M. J. Vicente Vacas, *Nucl. Phys. A* **705**, 90 (2002)
- [15] M. Post, S. Leupold and U. Mosel, *Nucl. Phys. A* **741** (2004) 81
- [16] H. A. Weldon, *Phys. Rev. D* **28**, 2007 (1983).



- [17] S. Ghosh, S. Sarkar and S. Mallik, Eur. Phys. J. C **70**, 251 (2010)
- [18] G. W. Semenoff and H. Umezawa, Nucl. Phys. **B 220**, 196 (1998)
- [19] A.J. Niemi and G.W. Semenoff, Ann. Phys. **152**, 105 (1994)
- [20] R.L. Kobes and G.W. Semenoff, Nucl. Phys. **B260**, 714 (1985)
- [21] S. Mallik and S. Sarkar, Eur. Phys. J. C **61**, 489 (2009).
- [22] T. Matsubara, Prog. Theor. Phys. **14** (1955) 351.
- [23] S. Ghosh, S. Sarkar and S. Mallik, Phys. Rev. C **83**, 018201 (2011).
- [24] R. D. Peccei, Phys. Rev. **176**, 1812 (1968).
- [25] H. Leutwyler, arXiv:hep-ph/9406283.
- [26] S. Mallik and S. Sarkar, Eur. Phys. J. C **25**, 445 (2002)
- [27] K. Nakamura *et al.* [Particle Data Group], J. Phys. G **37** (2010) 075021.
- [28] W. Rarita and J. Schwinger, Phys. Rev. **60**, 61 (1941)
- [29] M. Le Bellac, *Thermal Field Theory* (Cambridge University Press, Cambridge, 1996).
- [30] B. D. Serot and J. D. Walecka, Adv. Nucl. Phys. **16**, 1 (1986).
- [31] S. Sarkar, E. Oset and M. J. Vicente Vacas, Nucl. Phys. A **750**, 294 (2005)
- [32] P. Gonzalez, E. Oset and J. Vijande, Phys. Rev. C **79**, 025209 (2009)
- [33] L. D. McLerran and T. Toimela, Phys. Rev. D **31** (1985) 545.
- [34] P. Roy, A. K. Dutt-Mazumder, S. Sarkar, and J. Alam, J. Phys. G **35** (2008) 065106.
- [35] S. Sarkar, B. K. Patra, V. J. Menon and S. Mallik, Indian J. Phys. **76A** (2002) 385 [arXiv:hep-th/0010062].